INTERNAL MONITORING OF THE HL-LHC COMPONENTS

V. Rude*, H. Mainaud Durand†,
V. Barbarroux, P. Bestmann, J. Calmels, C. Petrone,
C. Cala Franco, M. Noir, M. Pentella, P. Sarvade, M. Sosin,
CERN, Geneva, Switzerland

Abstract

The High-Luminosity Large Hadron Collider (HL-LHC) project at CERN aims to enhance the LHC's performance and expand its potential for discoveries beyond 2029. New components will be installed within the 220 meters on either side of the collision points of the ATLAS and CMS experiments. This includes 16 Nb3Sn quadrupoles to focus the beam before the collision and 8 radio-frequency crab cavities to allow beam tilting, thereby increasing the number of collisions within experiments. Whether for quadrupoles or crab cavities, these elements consist of two distinct components: the visible outer envelope (called the vacuum vessel for quadrupoles and the cryomodule for crab cavities) and the active element installed inside (called the cold mass for quadrupoles and the cavity for crab cavities).

The HL-LHC project requires the determination of the position of the inner element within the outer envelope with an accuracy of ±0.1 mm (1σ). Previously, the position of the cold mass in a vacuum vessel was determined during construction and considered stable in warm conditions, with a thermal contraction model applied for cryogenic conditions. However, this assumption is no longer accurate enough for the stringent HL-LHC requirements. To determine the position of the inner element inside the outer envelope in real-time within the allowed tolerance of ±0.1 mm, the absolute distances between the two elements will be measured using multi-target Frequency Scanning Interferometry (FSI).

CERN has conducted tests on the first HL-LHC quadrupoles and crab cavities in warm and cold conditions, with the crab cavities monitored during their cooldown, and the position of the mechanical axis of the quadrupole cold mass compared with the behavior of the magnetic axis.

This paper will describe the monitoring system and report on the results from these initial measurements.

INTRODUCTION

In 2026, the HL-LHC project will start replacing nearly 1.2 km of the LHC accelerator, allowing for a ten-fold increase of integrated luminosity for the second decade of the LHC's operation [1]. The installation of new components, including 16 Nb_3Sn quadrupole magnets and 8 radio-frequency (RF) crab cavities, are critical corner stone of this upgrade. Both components are superconducting devices, where the Nb_3Sn quadrupoles have an enhanced magnetic field strength for focusing the beam, and the RF crab cavities are essential for beam manipulation to maximise luminosity.

* vivien.rude@cern.ch
† helene.mainaud.durand@cern.ch

For the alignment, more than one thousand sensors will be integrated through a Full Remote Alignment System (FRAS) [2], [3]. External monitoring will use 700 sensors to align the visible outer envelope of the components along the accelerator tunnel. Additionally, 320 sensors will be deployed for internal tracking, measuring the active elements installed within the visible outer envelope. Internal monitoring will cover the 16 Nb_3Sn quadrupoles and the 8 radio-frequency crab cavities.

The quadrupoles' outer envelope is referred to as the vacuum vessel, while their inner element is known as the cold mass (Fig 1).

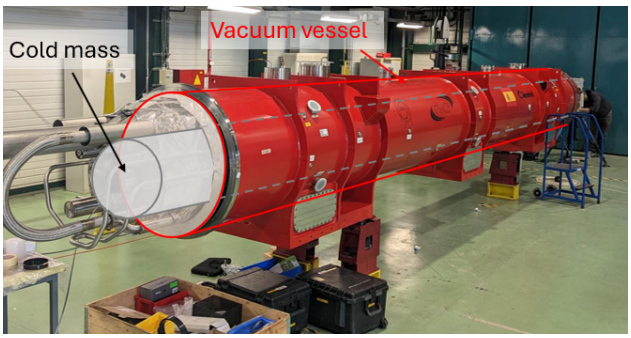

Figure 1: A Nb3Sn Quadrupole

Figure 2 illustrates the crab cavities with an outer envelope referred to as a cryomodule along with the two inner radio-frequency cavities [4].

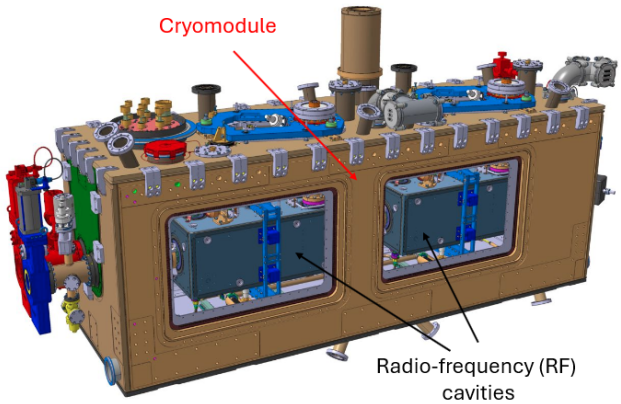

Figure 2: Internal monitoring for crab-cavities

The HL-LHC project requires that the position of the inner element within the outer envelope is determined with an accuracy of ±0.1 mm.

INTERNAL MONITORING SETUP

Acquisition System: FSI

The internal monitoring system employs Frequency Scanning Interferometry (FSI) [5], which measures the absolute distance between a fibre ferrule tip and a reflective target with a precision of a few micrometers over distances shorter than a meter (Fig 3) [6]. The interference beat frequency signal, resulting from the mixing of two optical signals: one reflected at the ferrule tip (acting as a semi-reflective mirror) and the other reflected from the target is analyzed. The beat frequency is proportional to the distance between the ferrule tip and the target. If the laser wavelength is swept at constant speed, the distance can be deduced using a Fourier transform technique [7].

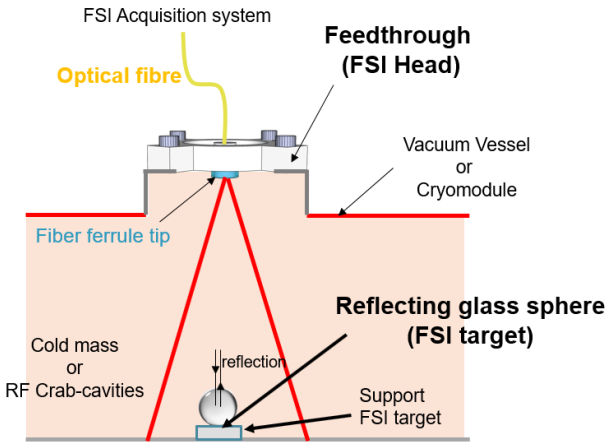

Figure 3: FSI Setup

Feedthroughs: FSI Heads

For internal monitoring, the fiber tip ferrule is a part of the FSI Head feedthrough, a leaktight interface between the component (under a secondary vacuum of 10^{-6} mbar) and the atmospheric pressure of the accelerator tunnel [8] (Fig 4).

Figure 4: FSI Heads: Left image shows one FSI Head for the quadrupole, and the right image shows one FSI Head for Crab-cavities

The inner position of the fiber tip ferrule inside the FSI head is measured during calibration with respect to external targets installed on the outer part of the feedthrough. After installation, these targets are measured with a laser tracker, determining the fiber tip ferrule's position within the component's coordinate system. The field of view of the quadrupole and crab cavity FSI heads differs due to the distance between the head and the target and the need to ensure sufficient optical power is reflected. The quadrupole FSI heads have a cone of vision of ±6 degrees, while the Crab cavity FSI heads have a narrower cone of ±2 degrees.

Reflectors: FSI Targets

The chosen FSI targets are 0.5" diameter, high refraction index glass spheres, engineered for micrometric precision. These spheres are partially coated with aluminium for detection by instruments like the AT960 Laser Tracker (Hexagon Metrology). They are installed on the internal component, and their position relative to the reference axis is determined before their installation inside the outer envelope (Fig 5). To resolve cryocondensation issues observed during initial tests in 2018, special FSI target supports providing cryo-condensation-free temperature conditions for the reflectors were developed [9] (cf. Fig. 5-left).

Figure 5: FSI Targets: Left image shows one FSI Target for the quadrupole, and the right image shows one FSI Target for Crab-cavities.

FSI Quadrupole Configuration

The cold mass is mounted on three feet inside the vacuum vessel, with four FSI measurements taken at each foot cross-section, totaling twelve observations. Each observation achieves a standard deviation of 0.040 mm, ensuring the position of the cold mass within the vacuum vessel is determined with an accuracy better than 0.1 mm (Fig 6). This 0.040 mm uncertainty accounts for the cumulative uncertainties of the FSI measurements, the position of the FSI targets relative to the cold mass reference axis, and the position of the FSI heads relative to the vacuum vessel reference axis.

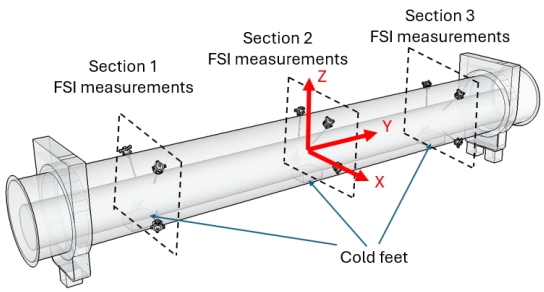

Figure 6: FSI Configuration for Quadrupoles

FSI Crab-cavity Configuration

The two RF cavities, enclosed in helium tanks, are suspended within the cryomodule. Eight FSI measurements per cavity determine their absolute position with respect to the cryomodule, with an accuracy of less than 0.1 mm (Fig 7). Each observation achieves a standard deviation of 0.040 mm.

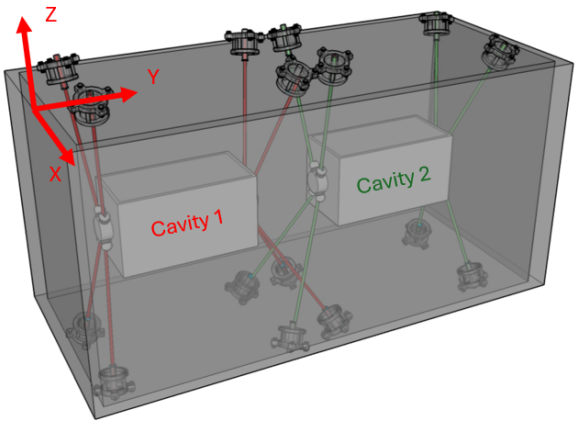

Figure 7: FSI Configuration for Crab-cavities

Fiducialization

Fiducialization is essential for aligning components to meet the required specifications. It involves measuring the relationship between a component's reference axis and external fiducials to ensure accurate alignment. The reference axis can be mechanical, magnetic, radio-frequency, or other.

For the cold mass, two reference axes are measured: the mechanical axis and the magnetic axis. The offset between these axes, determined during fiducialisation measurements, should remain constant, which is verified later in the paper.

In the case of the crab cavities, the reference axis is the cavity's internal radio-frequency axis. However, as it was not possible to directly measure this axis, it is approximated using the mechanical axis of the cavity, which is measured using a Coordinate Measuring Machine (CMM) during cavity assembly.

For the outer envelope (vacuum vessel or cryomodule), a mechanical axis is defined relative to its mechanical surfaces.

Cryostatting

Cryostatting involves positioning the inner element inside the outer envelope. During this step, a laser tracker is used to pre-adjust the inner component within the outer envelope. Following this, FSI measurements are conducted to determine the position of the inner component relative to the outer envelope, as the inner element is no longer accessible by the laser tracker.

QUADRUPOLES

This section summarizes the various displacements and deformations observed at each stage, from cryostatting to the cold state, for both the cold mass and the vacuum vessel.

Impact of Transport

After cryostatting, the cryostat (vacuum vessel + cold mass) was transferred to a dedicated facility for cold testing preparation. After the transfer, the position of the cold mass inside the cryomodule and the deformations of the components were measured. Although no significant shift between the two elements was detected, a vertical droop at each end was identified in both the vacuum vessel and the cold mass after transport (Fig 8).

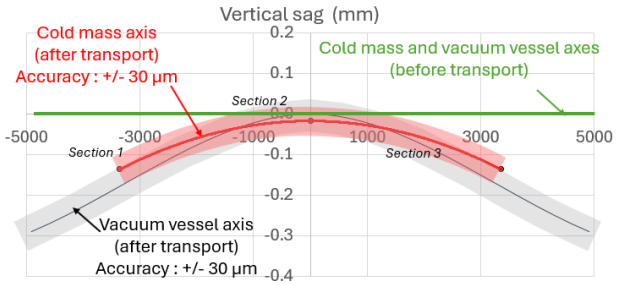

Figure 8: Vertical shape of the vacuum vessel and cold mass after transport

To better understand this deformation, a test was conducted using a single vacuum vessel installed with four different setup configurations. The shape of the vacuum vessel was measured at various temperatures using a laser tracker and modelled as a second-order polynomial. Figure 9 illustrates the vertical droop between the end sections (No. 1 and 3) and the middle section (No. 2). The deformation was found to include a random movement of up to 200 μm, and a temperature-correlated deformation of approximately 35 μm / °C. This behavior was consistent across six other cryostats that were also tested. To account for this deformation, the low-beta quadrupoles in the FRAS will be equipped with Wire Positioning Sensors (WPS) at the midpoint and at either end of the vacuum vessel to model this effect.

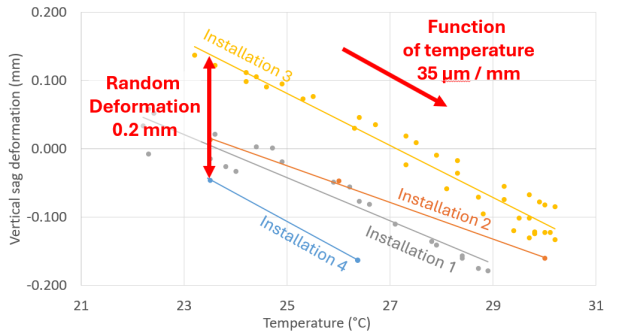

Figure 9: Vertical deformation after transport at different temperatures

Impact of Vacuum

The pressure inside the vacuum vessel is maintained at around 10^{-6} mbar to avoid heat transfer by conduction and convection from the cold mass. Figure 10 shows the simulated deformation of the vacuum vessel, with displacements reaching up to 80 μm. These simulations were confirmed by laser tracker measurements, particularly at the location of the FSI heads, where the largest deformations were observed. The deformation models will be applied to the FRAS for vacuum and cold conditions to ensure that each FSI observation between the FSI head and target remains within a standard deviation of 40 μm. It's important to note that during the pumping process, no significant movement of the cold mass inside the vacuum vessel was observed.

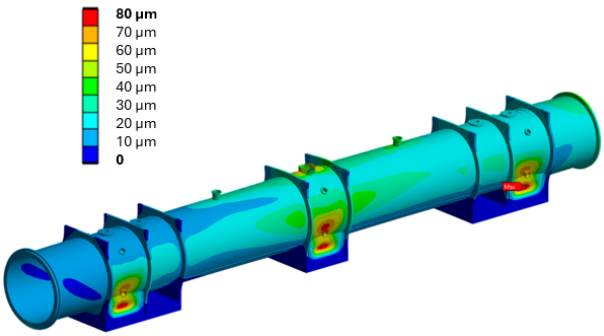

Figure 10: Deformation of the vacuum vessel due to vacuum pumping

Impact of Cool Down

FSI measurements were used to monitor the position of the cold mass inside the vacuum vessel during the cool down process, with data collected every 30 seconds on the quadrupole known as Q2a-P3. Figure 11 illustrates the vertical motion of the three sections of the cold mass as the temperature decreased from 295 K to 2 K. Vertical movements of 1.42 mm, 1.33 mm, and 1.56 mm were observed in sections 1, 2, and 3, respectively, with a measurement accuracy below 0.1 mm (1σ).

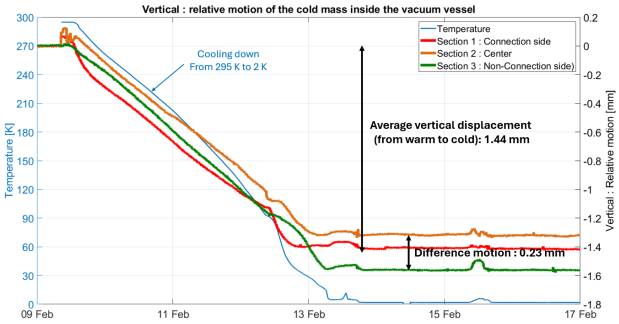

Figure 11: Relative vertical motion of the cold mass during cool down

A difference of 0.23 mm was observed between the vertical relative motion of the three feet during the cool down. This difference is attributed to variations in the composition of the feet. Testing of a few feet revealed a 10% difference in thermal contraction between warm and cold conditions (2 K).

Motion of the Magnetic and Mechanical Axes

For the quadrupoles assembled at CERN (Q2a and Q2b types), the magnetic axis was measured on the assembly bench at both warm and cold temperatures. The magnetic axis of the cold mass was determined by powering the magnet with a current of 5 A using sinusoidal excitation at a frequency of 9 Hz, using the Single Stretched Wire method (SSW) [10], [11], and achieving an accuracy of 0.1 mm (1σ). The cold mass, consisting of a magnet and a corrector, was analyzed along its length to determine the magnetic axis. The magnetic axis was then compared to the mechanical axis, which was reconstructed from FSI measurements.

Figure 12 presents the positions of the two axes at both warm and cold temperatures. The magnetic measurements revealed a vertical movement of 1.45 mm on the connection side (Conn) and 1.41 mm on the non-connection side (NConn). The average vertical displacement of both the mechanical and magnetic axes was consistent, measuring 1.44 mm and 1.43 mm, respectively. The difference between the magnetic and mechanical axes remained constant in both warm and cold conditions.

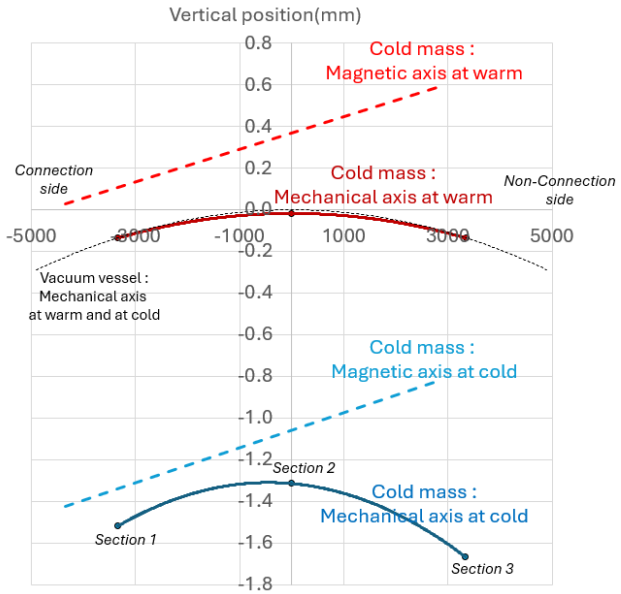

Figure 12: Comparison of magnetic and mechanical axes at warm and cold temperatures

No significant radial movement was detected between warm and cold conditions for either the magnetic or mechanical axis. The magnetic field direction was measured at both warm and cold temperatures with an accuracy of 0.1 mrad (1σ). No significant differences were observed in the direction of the magnetic field between the two temperature conditions.

CRAB CAVITIES

The crab cavity components presents significant technical and alignment challenges due to several factors:

- Pumping: Reducing the pressure from 1 bar to 10^{-6} mbar alters the cryomodule's shape by up to 1 mm.
- Cool down and Pumping: Both processes shift the position of the two cavities inside the cryomodule by up to 1 mm.
- Complex Movements: The cavities exhibit movement not only in the radial and vertical directions but also in pitch and yaw.
- Non-compensatable misalignment: With two cavities installed inside the cryomodule, misalignment of the active elements cannot be corrected solely by adjusting the outer envelope.
- Anticipating Deformations: Alignment must be performed at ambient pressure while accounting for deformations observed during previous phases, such as pumping and cool down.
- Alignment Uncertainty: A standard deviation of 40 μm should be reached on each FSI observation between the FSI head and the FSI target.

The first crab cavity prototype was assembled by the STFC in the UK, with reception tests conducted at CERN in late 2023. The prototype was subsequently installed in a bunker for cold testing. Three cold test cycles were performed, allowing the measurement of various deformations and movements under ambient pressure, vacuum, and cold conditions. The repeatability of these cycles allowed for a direct comparison between simulated results and actual real-world behaviour.

Impact of Vacuum

Figure 13 illustrates the simulated deformation of the cryomodule due to vacuum pumping.

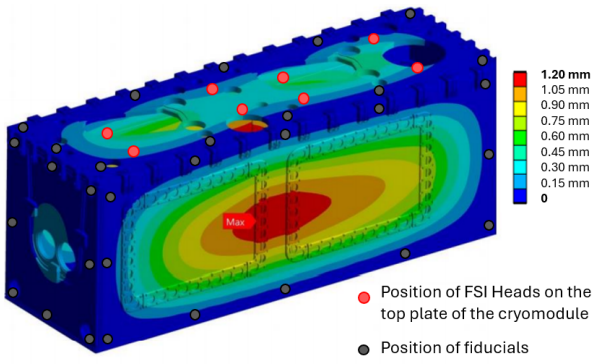

Figure 13: Deformation of the cryomodule due to vacuum pumping

The fiducials on the cryomodule were installed along the edges of the least-deforming areas. Across all states — ambient pressure, vacuum, and cryogenic temperature — the fiducials returned to the same position with an accuracy of less than 40 μm (rms: 10 μm). The FSI heads, installed in areas of significant deformation (up to 0.4 mm), also returned to their original positions with an accuracy of better than 50 μm (rms: 15 μm) for each state.

Table 1 shows that while pumping down the cryostat the crab cavities moved radially by 0.40 mm and vertically by 0.42 mm, with additional rotations including a roll angle of 0.63 mrad and a pitch angle of 0.15 mrad. During the three pumping cycles, the same movement of the two cavities inside the cryomodule was observed, with a repeatability of better than 0.05 mm in both the radial and vertical directions.

Table 1: Movement of the cavities due to pumping

	Movement	**Accuracy**
Radial : Tx (mm)	**0.40**	<0.10
Longitudinal : Ty (mm)	-0.02	0.10
Vertical : Tz (mm)	**-0.42**	<0.10
Pitch : Rx (mrad)	**0.15**	0.04
Roll : Ry (mrad)	-0.63	0.40
Yaw : Rz (mrad)	-0.01	0.10

Impact of Cool down

Figure 14 shows the cryomodule's deformation due to cool down, measured by a laser tracker. Deformations of up to 0.1 mm were observed on the cryomodule's top plate.

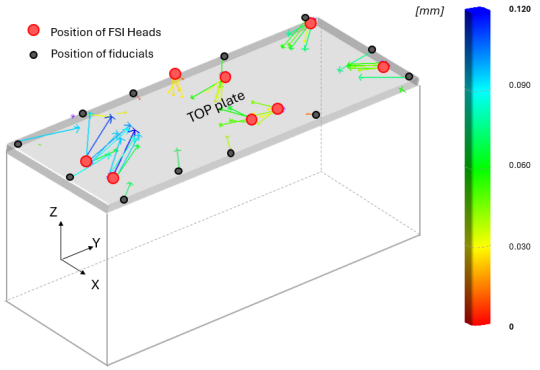

Figure 14: Deformation of the top plate of the cryomodule when cool down

After analysis, this thermal contraction was primarily caused by thermal convection between the thermal screen (40 K) and the top plate (300 K). The thermal screen is supported by four blades located beneath the top plate, leading to a temperature drop of approximately 5 K on the top plate. The scale factor derived from measurements on the stainless steel top plate corresponds to a temperature variation of 6 K, in agreement with simulated convection.

Table 2 details the cavity movements during cool down. A yaw angle of 0.38 mrad and a radial translation of 0.19 mm were observed. In the vertical direction, the cavities shifted by 1.18 mm, with a pitch angle of 0.17 mrad. Thermal

contraction due to the temperature difference between warm and cold (2.6 mm per meter) was also measured. The behaviour of the two cavities was consistent within 0.1 mm.

Table 2: Movement of the cavities due to cool down

	Movement	Accuracy
Radial : Tx (mm)	**0.19**	<0.10
Longitudinal : Ty (mm)	-0.10	0.10
Vertical : Tz (mm)	**1.18**	<0.10
Pitch : Rx (mrad)	**-0.17**	0.04
Roll : Ry (mrad)	0.29	0.40
Yaw : Rz (mrad)	**0.38**	0.10
Scale factor (mm/m)	**-2.60**	0.25

Pre-alignment of the cavities at warm and ambient pressure must consider the cryomodule deformation and the cavity movements. Figure 15 summarizes the vertical displacement of the cavities from pre-alignment at ambient pressure to their final positions at cold.

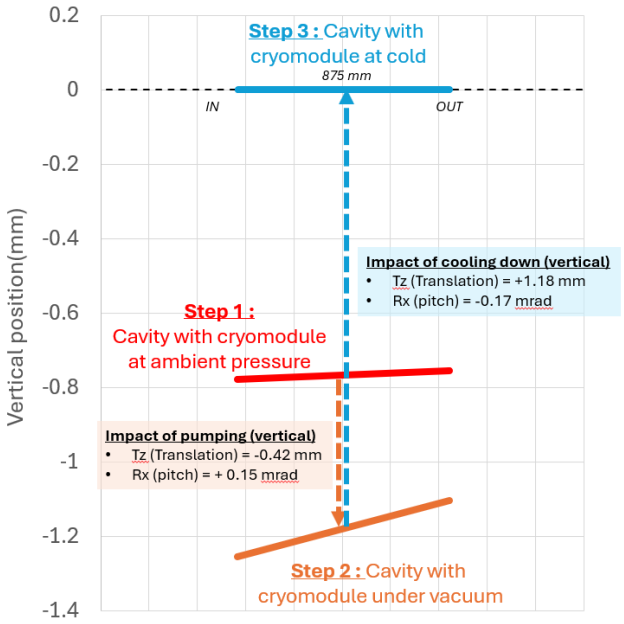

Figure 15: Vertical displacement of the cavities during cool down

Alignment must be performed at ambient pressure, and ensuring the correct positions of the two cavities with an accuracy of 0.1 mm at cold is a significant challenge. However, the experience gained from three cool down cycles has increased confidence in achieving this goal.

In December 2024, the RFD prototype cryomodule will be installed in the SPS accelerator, providing an opportunity to test the impact of transport and apply the experience gained. Additionally, the position of the radio-frequency axis will be analysed using the beam, confirming the alignment and validating the assumption that the radio-frequency axis can be approximated to the mechanical axis of the cavity structures.

CONCLUSION

During the cold tests of the first HL-LHC components, internal monitoring provided significant insights into the internal movements of the cold components. Despite the large deformations caused by vacuum pumping, the outer envelope's shape could be modelled with a precision of 0.04 mm RMS. Measurements taken under different conditions of pressure and temperature confirmed that the outer envelope's deformation is repeatable with a deviation of less than 0.04 mm. The use of Frequency Scanning Interferometry (FSI) allowed a highly accurate determination of the position of the inner elements relative to the outer envelope, achieving positional accuracy of less than 0.1 mm in both radial and vertical directions.

For the quadrupoles, the relationship between the mechanical and magnetic axes was shown to remain consistent for both warm and cold temperatures, thanks to the stability of the alignment and internal monitoring system.

For the crab cavities, the behaviour of the two cavities could be shown to be consistent within 0.1 mm using the internal monitoring system. The upcoming installation in the SPS accelerator in December 2024 offers an opportunity to gather additional experience with a fully operational system before proceeding with the implementation of internal monitoring in the eight series modules.

REFERENCES

[1] I. Béjar Alonso et al., *High-Luminosity Large Hadron Collider (HL-LHC): Technical Design Report*, CERN, CERN Yellow Reports: Monographs, 2020. https://doi.org/10.23731/CYRM-2020-0010

[2] V. Barbarroux et al., *Full Remote Alignment System, Engineering specification*, CERN, CERN reference: LHC_-ES0049, Geneva, 2024.

[3] H. Mainaud Durand et al., *Full Remote Alignment System for the High-Luminosity Large Hadron Collider*. In Proc. of IWAA, Stanford, United States, 2024.

[4] R. Calaga et al., *First demonstration of the use of crab cavities on hadron beams*. Physical review accelerators and beams, 2021.

[5] M. Sosin et al., *Frequency Sweeping Interferometry for Robust and Reliable Distance Measurements in Harsh Accelerator Environments*. In Proc. of SPIE Optics + Photonics, San Diego, United States, 2019.

[6] J. Calmels et al., *Comparison of FSI Measurement and CMM Measurement*. EDMS 3090900, CERN Document, Geneva, 2024. https://edms.cern.ch/document/3090900/1

[7] M. Sosin et al., *A Multichannel Frequency Scanning Interferometry System for Large Scale Metrology of Accelerator Components*. In Proc. of IPAC, Nashville, United States, 2024.

[8] M. Sosin et al., *Robust Optical Instrumentation for Accelerator Alignment Using Frequency Scanning Interferometry*. In Proc. of IPAC, Campinas, Brazil, 2021.

[9] F. Micolon et al., *Thermal Engineering of Optical Mirrors for Use at Cryogenic Temperature Inside a LHC Magnet Cryostat*. In Proc. of CEC/ICMC, Hartford, United States, 2019.

[10] C. Petrone, *Wire methods for measuring field harmonics, gradients, and magnetic axes in accelerator magnets*. Ph.D thesis, 2013.

[11] M. Pentella et al., *Field-axis measurement of an AC-powered magnet by a single-stretched wire*. IMEKO XXIV World Congress, Hamburg, 2024.